www.pnas.org/cgi/doi/10.1073/pnas.1911240117

PNAS
www.pnas.org

Supplementary Information for

Transcranial Magnetic Stimulation Induced Perturbations of Resting-State-Networks are Reproducible Markers of Causal Network Dynamics

Recep A. Ozdemir[1], Ehsan Tadayon[1], Pierre Boucher[1], Davide Momi[1], Kelly A. Karakhanyan[1], Michael D. Fox[1,2], Mark Halko[1], Alvaro Pascual-Leone*[1,3], Mouhsin M. Shafi*[1], Emiliano Santarnecchi*[1,4]

Emiliano Santarnecchi
Email: esantarn@bidmc.harvard.edu

This PDF file includes:

Supplementary methods and Results
Figures S1 to S4
Legends for Movies S1
SI References

Other supplementary materials for this manuscript include the following:

Movie SV_1
Movie SV_2

Supplementary Methods

Resting-state fMRI data and preprocessing

Briefly, structural T1-weighted processing included surface reconstruction using Freesurfer, spatial normalization, brain extraction and tissue segmentation (white-matter, gray-matter and cerebrospinal fluid (CSF)). Functional data were slice time corrected and motion-corrected and registered to the T1-weighted structural MRI using boundary-based registration with six degrees of freedom. CompCor approach (with six temporal and six anatomical components) was deployed for physiological noise regressions, and the time series were bandpass filtered (0-008 - 0.08). The time-series were resampled onto fsaverage4 for creating individualized networks.

Generating individual networks

First, group-average functional networks are morphed into the subject's cortical surface using surface-based registration. Then, using the subject's preprocessed resting-state fMRI data, the vertices are re-assigned to one of the 18 networks in an iterative procedure based on the correlation between each vertex and the average time-course for each network while considering the variability of each network across subjects (i.e. confidence map). Networks #15-17 were combined to get DMN, and Networks #5 and #6 were combined to get DAN (SI Appendix, Fig. S4).

Sandia Matrices

SM is a recently developed PC-based, matrix-like abstract reasoning task resembling and expanding the Raven's Matrices (Raven and Court, 1998). Compared to the original Raven stimuli, the SM tool includes multiple sets of validated stimuli which allow for repeated measurement of g*f*, while allowing for sensitive recording of response times (Santarnecchi et al., 2016, 2013). Each matrix is composed of a 3x3 grid, with each cell in the grid containing a set of shapes. A blank cell is present in position 3–3 of the grid (bottom right). Participants were required to complete the matrix using one of eight options. Participants responded by pressing the corresponding key on a keyboard (1-8). A maximum of 60 seconds was given for each matrix to be completed, after which the next matrix appeared. Two different sets of matrices were presented: Relational matrices (g*f* relational) and Logic matrices (g*f* logical). Relational matrices could be solved by capturing variations in the features of shapes across cells in the grid, (i.e., color, size, orientation, number, shape), with some features staying constant while others vary. Logic matrices required participants to perform logical operations across the matrix (i.e., conjunction, disjunction, or exclusive disjunction, known as AND, OR and XOR functions, respectively), similarly to the conditional inferences discussed above. Logic and relational matrices were presented in a randomized order, and the interstimulus interval was 5 seconds. Additionally, before starting the first block, participants performed a short training exercise to familiarize with the stimuli and reduce possible novelty effects in the first block. Before starting the training block, brief verbal instructions were given to participants explaining the task. Following

training participants completed 12 trials of both Relational and Logic matrices presented in a randomized order (24 matrices in total, with each matrix appearing for 60 sec),

TOPF

The TOPF provided an estimate of premorbid intellectual abilities. Participants were requested to read aloud a total of 70 words, focusing on pronunciation. An estimated premorbid IQ score was calculated based on the number and type of errors. The test has been used in multiple cognitive studies (Alves et al., 2013) and clinical trials (Berg et al., 2016), providing a brief, validated estimate of IQ.

SRTT

A visual cue was presented at four different positions, configured horizontally at the center of a computer screen. Subjects were asked to press the response button corresponding to the position of the visual cue as quickly as possible. The visual cues were presented either in a repeating sequence or in a random order. In the sequenced trials, the location of the stimulus followed a fixed order, while in random trials the stimuli were presented in random locations. When the task was finished, a questionnaire was fulfilled where participants were asked to indicate whether the visualization pattern was based on a repeated sequence or not. Subjects were unware about the questionnaire before the task.

EMG Data Processing

EMG data were amplified and digitized using a Powerlab 4/25T data acquisition system (ADInstruments) at a sampling rate of 4000 Hz (bandpass filtered at 10Hz to 2000Hz). EMG signals were continuously streamed by using LabChart software (LabChart 8.0) to monitor MEPs and epochs were recorded with a 150ms window length covering from 50 ms before to 100 ms after TMS pulse.

E-Field modeling

The e-fields were simulated using SIMNIBS (v2.1) software. The head models were reconstructed using *mri2mesh* pipeline, which creates tetrahedral meshes consisting of white-matter (WM), gray-matter (GM), CSF, skull and scalp. We used the default conductivity values of 0.126 S/m for WM, 0.275 S/m for GM, 1.654 S/m for CSF, 0.01 S/m for the skull, and 0.465 S/m for scalp. We measured dI/dt from the Magventure Machine based on the stimulus intensity. The calculated E-fields were normalized by the maximum value of E-fields for each stimulation target. The normalized E-field maps were mapped to the fsaverage common template and averaged across subjects for visualization purposes.

EEG data Processing

First, the two separate blocks of 60 trials were merged to create a single block of 120 trials. The merged trials were then segmented into 3000ms epochs, each starting 1000ms before (pre-stimulus) and ending 2000ms (post-stimulus) following TMS pulse,

respectively. Baseline correction was performed by subtracting the mean pre-stimulus (-900 to -100) signal amplitude from the rest of the epoch in each channel. Following baseline correction, data were visually inspected to identify extremely noisy channels with high amplitudes (3 ± 2 channels were deleted on average; range 0–6 out of 63. See Figure S1 step 3 for a sample). Zero-padding between -2ms and 14ms time range were then applied to remove the early TMS pulse artifact from the EEG data. All zero padded epochs were then tagged based on voltage (≥100 μV), kurtosis (≥ 3), and joint probability (Single channel-based threshold ≥ 3.5sd; All channel-based threshold ≥ 5sd) metrics to identify excessively noisy epochs. Visual inspection was performed on the tagged epochs for the final decision for the removal of noisy epochs (24 ± 10 epochs were deleted on average; range 2-44 out of 120; See Figure S1 steps 4 and 5 for a sample). Next, an initial round of fast independent component analysis (fICA) (43) was performed to exclusively identify and remove components with early TMS evoked high amplitude electrode and EMG artifacts (1± 1 components were removed; range 0-3 out of 60, See Figure S1 step 6 for a sample). Prior to the first round of fICA, the EEG data were reduced into 60 dimensions by using principal component analyses (PCA) to minimize overfitting and noise components. After the first round of fICA, the EEG data were interpolated for previously zero-padded time window around TMS pulse (-2ms to 14ms) using linear interpolation, band pass filtered using a forward-backward 4th order butterwoth filter from 1 to 100Hz, notch filtered between 57 and 63Hz, and referenced to global average (See Figure S1 step 7 for a sample data set). Subsequently, the data were reduced into 57 dimensions using PCA, and a second round of fICA was run to manually remove all remaining artifact components [4] including eye movement/blink, muscle noise (EMG), single electrode noise, TMS evoked muscle, cardiac beats (EKG), as well as auditory evoked potentials (22± 6 components were removed; range 18-28 out of 37, See Figure S1 step 8 for topography, time series and power spectrum of representative artifact components). In both rounds of fICA, a semi-automated artifact detection algorithm incorporated into the open source TMS-EEG Signal Analyzer (TESA v0.1.0-beta) extension for EEGLAB was used to classify and visually inspect components based on their frequency, activity power spectrum, amplitude, scalp topography, and time course (44) (http://nigelrogasch.github.io/TESA/). Finally, the data were low pass filtered with a 4th order Butterworth filter at 50Hz, and interpolated for missing/removed channels using spherical interpolation (See Figure S1 step 9 for a sample cleaned data set with topography of selected TMS evoked potentials).

GMFP and LMFP

Global cortical activation level following TMS of DMN and DAN was measured with Global Mean Field Power (GMFP) analyses on TEPs using the following equation.

$$GMFP(t) = \sqrt{\left\{\frac{\sum_i^k (\mathrm{V}i\ (\mathrm{t}) - \mathrm{V}_{mean(t)})2}{K}\right\}}$$

Where $V_i(t)$ is the voltage at electrode *i* at a certain point in time, $V_{mean(t)}$ is the mean of instantaneous TEP across electrodes, and *K* is the number of electrodes. The GMFP can be used to measure the global brain response to TMS (Lehmann and Skrandies, 1980; Komssi et al, 2004). A Local Mean Field Power (LMFP) analysis was also performed to identify local changes in cortical excitability induced by TMS of DMN and DAN. Region of Interests (ROIs) were determined separately for each hemisphere from the selected channels over frontal (Right Frontal 'RF' electrodes: FC2, FC4, FC6, F2, F4, F6 and Left Frontal 'RF' electrodes: FC1, FC3, FC5, F1, F3, F5), motor (Right Motor 'RM' electrodes: C2, C4, C6 and Left Motor 'LM' electrodes: C1, C3, C5), parietal (Right Parietal 'RP' electrodes: CP2, CP4, CP6, P2, P4, P6 and Left Parietal 'LP' electrodes: CP1, CP3, CP5, P1, P3, P5) and visual cortices (Right Visual 'RV' electrodes: PO4, PO8, O2 and Left Visual 'LV' electrodes: PO3, PO7, O1). LMFP was calculated as root-mean-square value of the ROI electrodes for each time point (Casarotto et al., 2013).

TEP time series were used to test reproducibility of TMS evoked global and local cortical responses in electrode space.

Supplementary Results

DMN stimulation induces higher global cortical activation in the resting brain.

GMFP time series for a representative subject, comparison of group mean GMFP time series with standard deviations for DMN and DAN stimulations, and individual sum of GMFP values, computed as the total amount of cortical activation from 0 to 400ms post TMS, with trend lines were provided in supplementary figure $S2A_1$, $S2A_2$ and $S2A_3$ respectively. We first computed cluster-based permutation (permutation n=10000) paired t-test statistics (Maris and Oostenweld, 2007) on GMFP time series at each time point from -200 to 400ms to compare temporal evolution in global cortical activation between DMN and DAN stimulation. Although DMN stimulation has higher values (Figure $S2A_2$), cluster-based permutation pairwise comparisons did not reveal significant differences ($p > 0.05$) at any time point between DMN and DAN. However, pairwise comparison for individual sum of GMFP values showed that DMN simulation resulted in increased global cortical excitability ($p = 0.03$) within 400ms window following TMS, when compared to DAN stimulation (Figure $S2A_3$), suggesting that, at the group level, total amount of global cortical activation was higher following DMN stimulation in the resting brain. Given high inter-individual variability in sum of GMFP values (See shaded regions in figure $S2A_2$) and a recent study (Jannati et al., 2017) showing the BDNF polymorphism as potential confounder in TMS induced responses, we split our participants into two groups based on their BDNF polymorphism (Val66Met vs Val66Val), and compared their GMFP values both for DAN and DMN stimulation (Figure S2). Independent sample t-tests revealed no significant differences between groups ($p > 0.05$). Additionally, we ran control analyses to further examine whether higher GMFP values following DMN stimulation is confounded with possible different muscle activation patterns across stimulation conditions due to more medial or lateral targeted brain regions. Given the proximity of DMN stimulation targets to scalp/neck muscles we carefully inspected the systematic presence of stronger muscle activations following DMN stimulation which might potentially startle the subjects and thus potentially induce saliency-related Event-Related-Potentials. An additional cycle of

ICA analyses was ran using all session-1 data sets for each participant, by systematically keeping the TMS induced muscle components while removing all other components from the data. Supplementary figure S3 below shows examples of TMS induced muscle components for a representative subject (and for both stimulation conditions) that were kept in the data. We then quantified the amplitude of TMS induced muscle responses with GMFP analyses (figure S3B). Analysis of time series (Figure S3B, left panel) and overall response (figure S3B, right panel) showed highly similar and non-significant differences between stimulation conditions ($p > 0.05$), suggesting that there is no systematic presence of significantly stronger muscle responses during DMN stimulation.

Similar to GMFP time series analyses, permutation based pairwise comparisons for LMFP time series also failed to reveal significant differences at any time point for all ROIs ($p > 0.05$), although the DMN time series were higher in general (Supplementary Figure $S4B_2$). Pairwise comparisons for individual sum of LMFP values did not show any significant differences ($p > 0.05$) between DMN and DAN stimulation for the total amount of local cortical activations at any ROIs (Figure $S4B_3$).

Test re-test reliability of TEPs

To test the reproducibility of TMS evoked cortical activation dynamics, we first generated grand mean TEP time series, computed as the mean time series of all participants, for each EEG channel across stimulation conditions (DMN vs DAN) and sessions (Session-1 vs Session-2) (Figure S6A shows TEPs for DAN and Figure S6B shows TEPs for DMN). We then computed the Pearson correlations across grand mean TEP time series at every 100ms windows from -100ms to 700ms after TMS. Topographical evolution of these correlations are provided in figure S6C for each 100ms window. Scalp map topographies for pre-stimulus window (-100 to 0ms) showed predominantly low negative correlations ($r < 0.5$), in both stimulation condition across sessions. For the DAN stimulation while increased positive correlations were mainly observed over bilateral prefrontal and left medial parietal cortices (r range: 0.11-0.89) 100ms following TMS, highest positive correlations across DAN sessions were achieved between 101-200ms and 201-300ms windows for the entire scalp (r range: 0.56-0.99), except electrodes over central parietal region close to stimulation site (CP1: r=0.29, and CPz: r=0.44). Positive correlations notably diminished after 300ms and returned to pre-stimulus values 500-600ms following TMS. For the DMN stimulation positive correlations mainly rose bilaterally over temporal-parietal, visual, motor and pre-motor cortices in the first 100ms window (r range: 0.64-0.93) and peaked between 101-200ms and 201-300ms windows following TMS (r range: 0.79-0.99), except in temporal parietal electrodes that are closer to stimulation site (C6: r=0.37, and CP6: r=0.51). Contrary to the DAN stimulation, positive correlations following DMN stimulation survived up to 600ms window especially over frontal cortices and returned to pre-stimulus values 600-700ms following TMS. Comparison of global cortical correlation values, computed as the grand mean of all scalp electrodes, between the DAN and DMN stimulation revealed significantly higher correlations for the DMN scalp maps at 301-400ms ($p = 0.02$), 401-500ms ($p = 0.03$) and 501-600ms ($p = 0.01$) windows, suggesting prolonged reproducibility in TEPs following DMN stimulation (Figure S6D).

Supplementary Figures

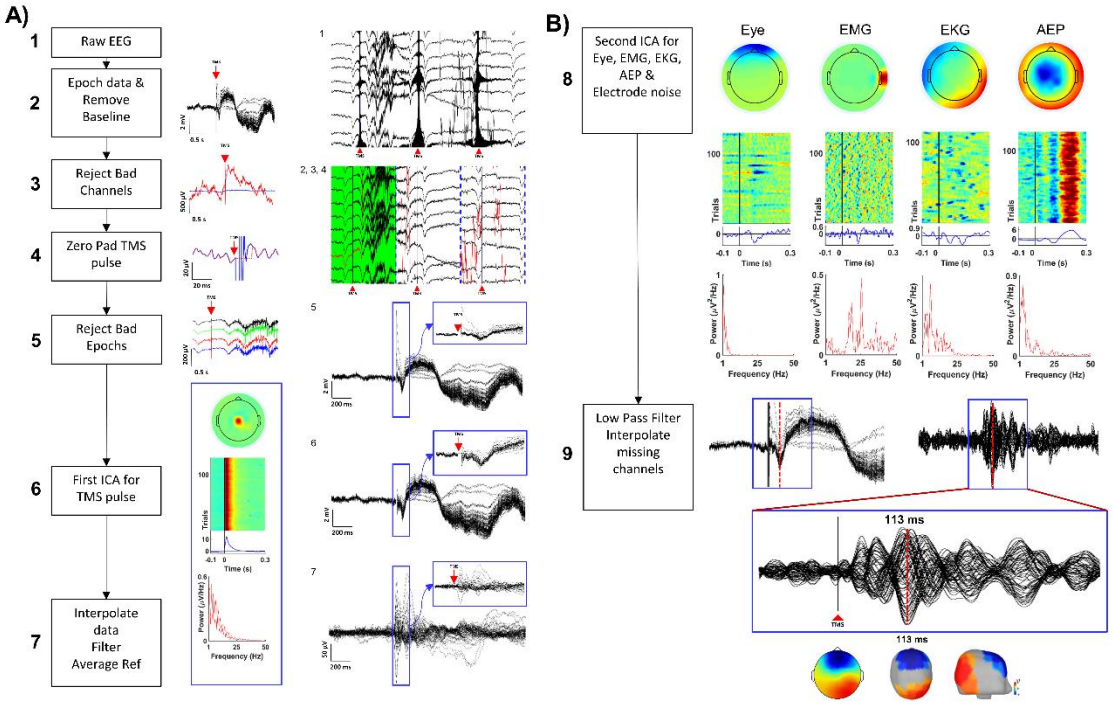

Supplementary Figure 1. EEG Signal Preprocessing: This supplementary figure shows major steps of EEG data cleaning procedures on a sample data set (panel A and B), and resulting signal transformation showing evolution of TMS evoked potentials (TEPs), with final scalp topography of a selected TMS evoked potential peak (Step 9). See methods for details.

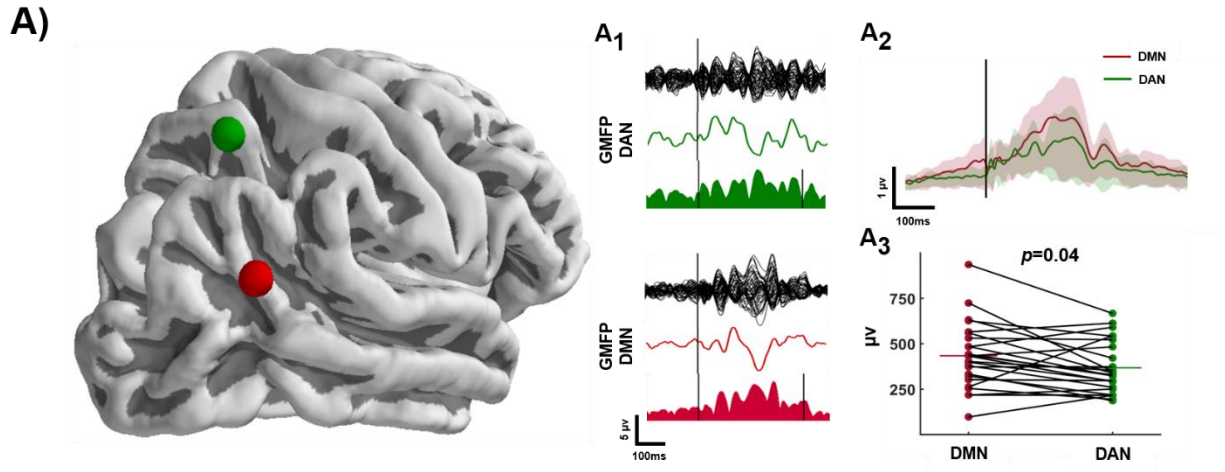

Supplementary Figure 2. TMS targets for DAN (green circle) and DMN (red circle) were shown in Panel A for a representative subject. TEPs (black lines representing each EEG electrode) and grand mean (solid colored lines) of all electrodes with resulting GMFP time series (colored areas under the integrated grand mean curves) were shown in Panel A_1. Group means (solid lines) and standard deviations (shaded regions) of GMFP time series for each network stimulation were shown in panel A_2. The area-under-the-curve of individual TMS evoked GMFPs (colored dots) and grand means (solid colored lines) of DAN and DMN stimulation along with between network comparison statistics were shown in Panel A_3 (Individual trends in TMS evoked GMFPs, as a function of network stimulation, were shown with solid black lines connecting each individual's GMFP values across stimulation conditions. Note that DMN stimulation induces significantly (p=0.04) higher global electro-cortical activity at the group level, when compared to DAN stimulation).

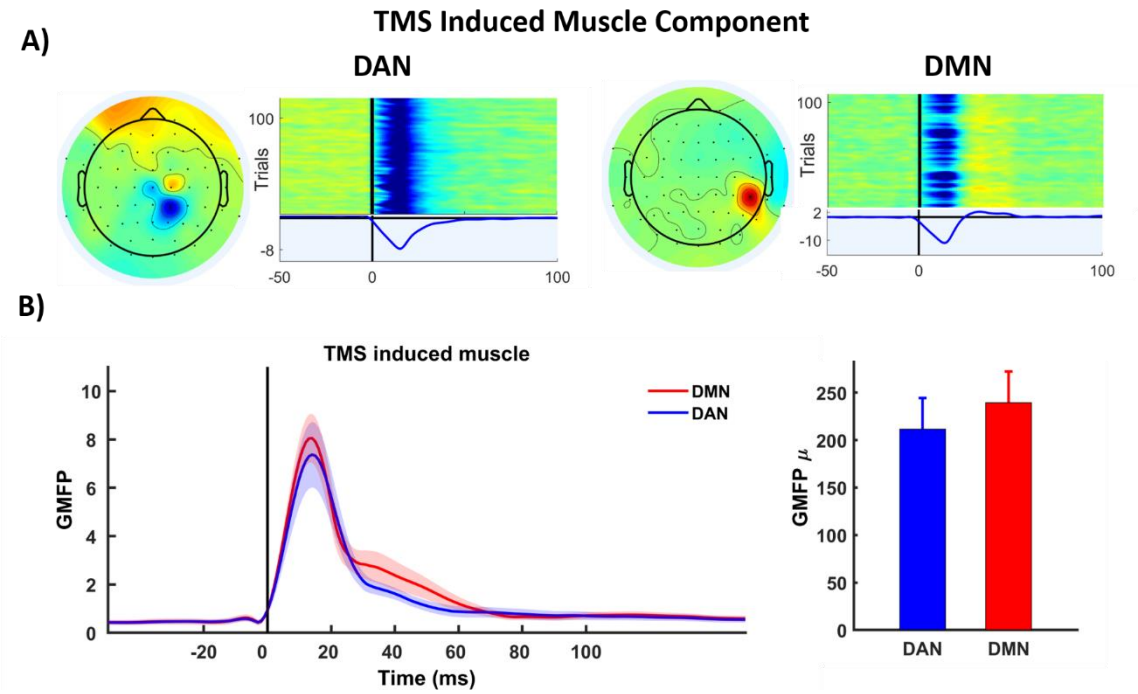

Supplementary Figure 3: TMS induced muscle components. (A) Examples of TMS induced muscle components from a representative subject for both stimulation conditions (DAN: left panel, DMN: right panel). (B) Group averaged GMFP time series (left panel) for TMS induced muscle components (DAN: Blue solid line, DMN: red solid line with corresponding shaded regions representing standard error of mean), and sum of GMFP activity (right panel) for 100ms following TMS.

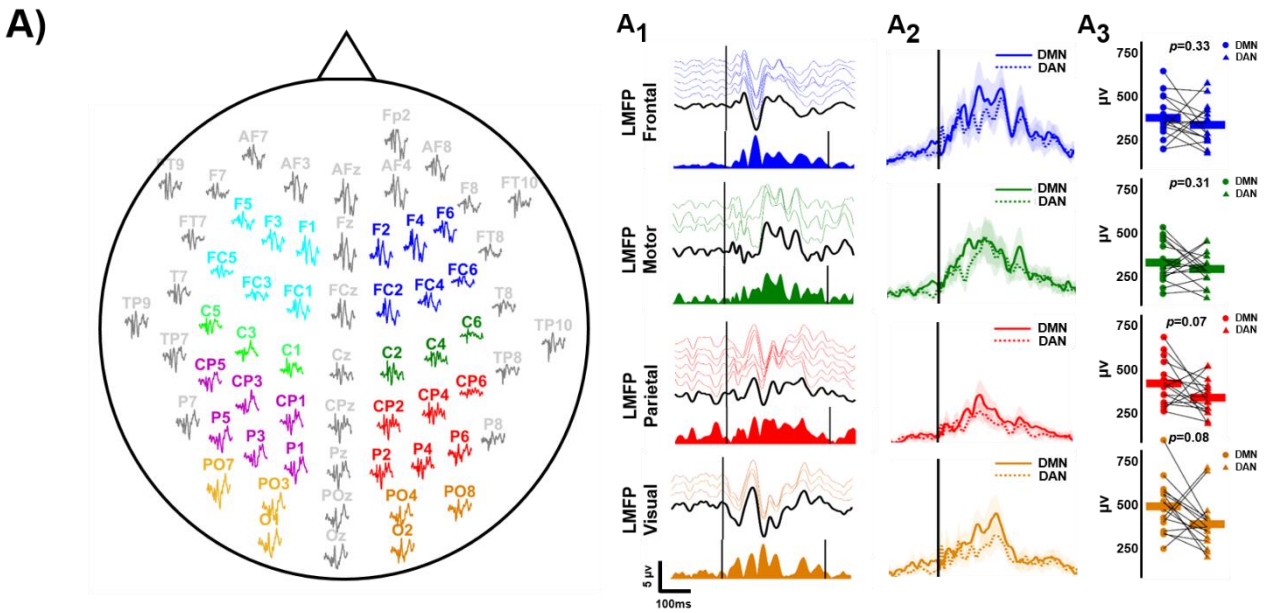

Supplementary Figure 4. (A) Color codes of selected EEG electrode groups for LMFP computations in each ROI. Dark colored channels represent frontal (blue), motor (green), parietal (red) and visual (brown) ROIs for LMFPs on the right hemisphere (stimulated), respectively. Corresponding light colored channels represents left hemisphere ROIs for LMFPs. LMFP profiles of stimulated hemisphere for a representative subject, Grand mean LMFP time series (colored solid lines) with standard deviations (color shaded regions), and individual TMS evoked LMFP values of each network stimulation along with between network comparison statistics were shown in Panels A_1, A_2, and A_3, respectively.

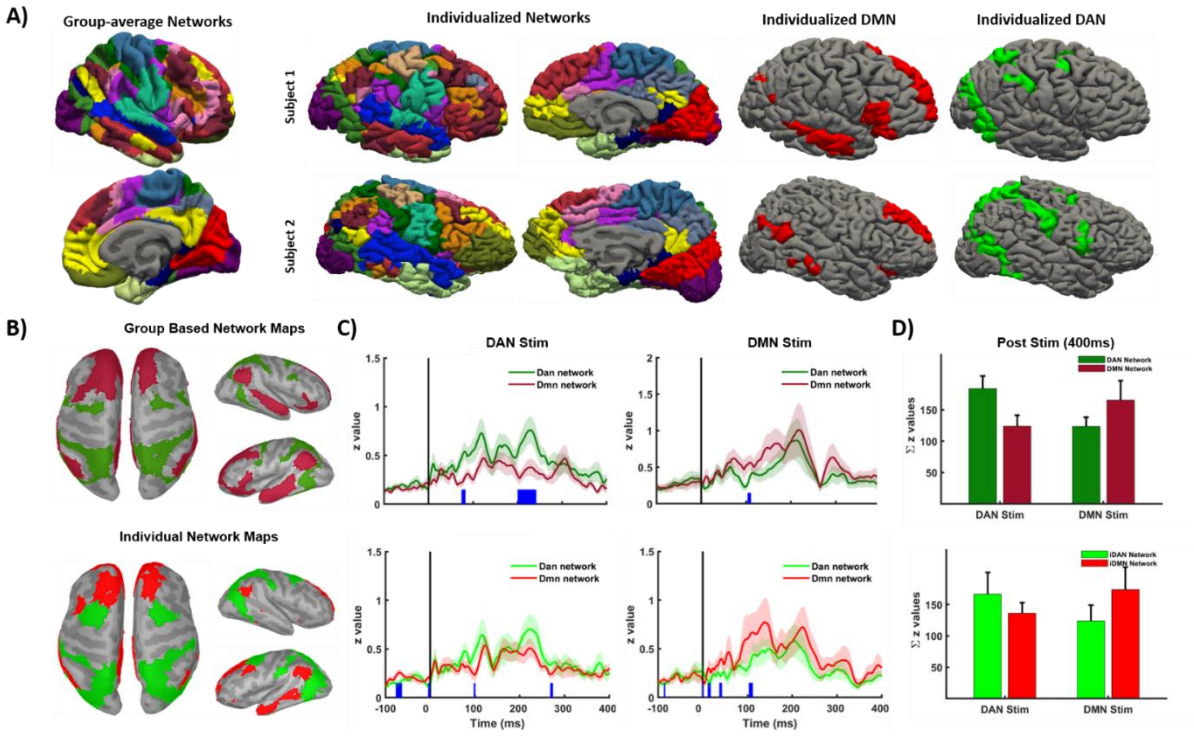

Supplementary Figure 5. (A) Individualized Networks. Group-average functional networks are morphed into subject's anatomy and through an iterative process the vertices are assigned to the network that they have the highest correlation with. The individualized networks as well as the individualized DMN and DAN are shown for two representative subjects. (B) Group-based (upper panels) and individual network maps (lower panels) on a common template. (C) Comparison of group averaged current density time series across stimulation conditions extracted both from group-based (upper panel) and individual (lower panels) network maps. (D) Sum of overall network activity 400ms following TMS across stimulation conditions.

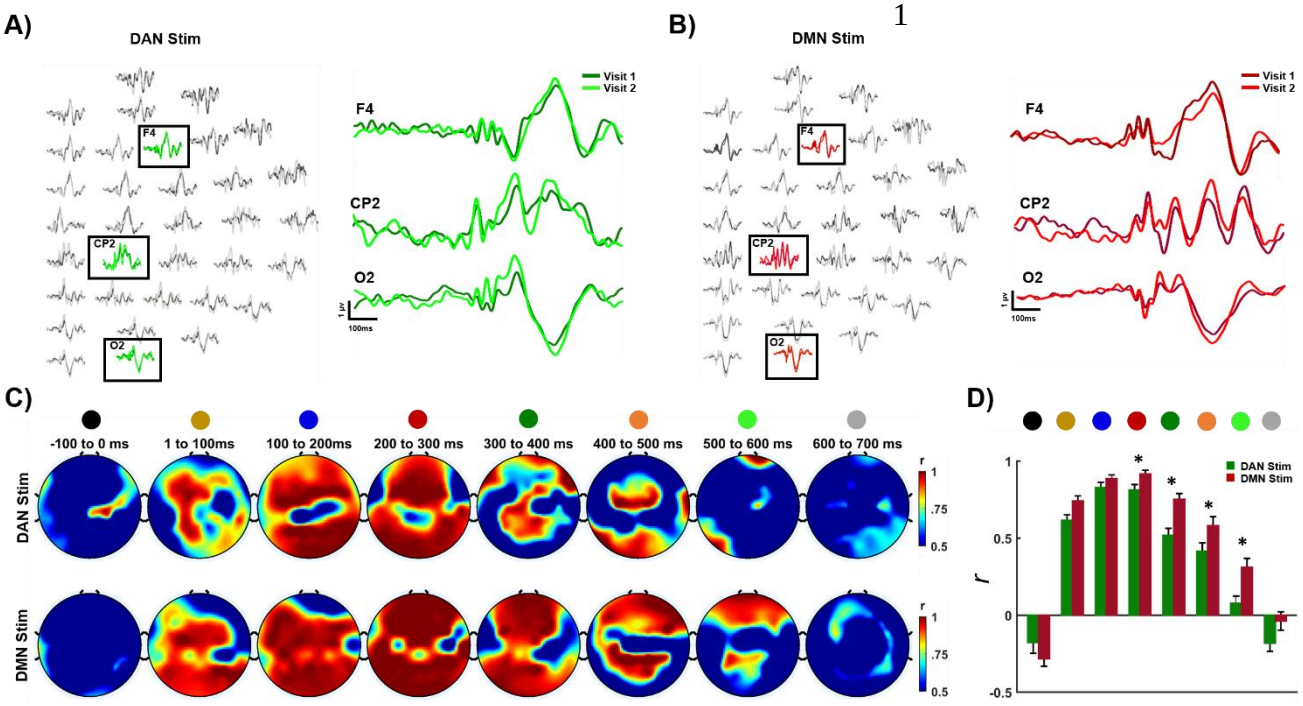

Supplementary Figure 6: Topographical similarity of TEPs between two identical TMS sessions (Reliability of TEPs): Grand mean TEP time series of EEG electrodes on the right (stimulated) hemisphere following DAN (panel A) and DMN (Panel B) stimulation across sessions (black solid lines show TEPs recorded in visit-1 while gray solid lines shows TEPs recorded in visit 2). Colored time series are expanded and presented on the right side of Panels A and B to show time course of representative channels from frontal (F4), parietal (CP2) and visual (O2) cortices across visits. Topography of test re-test correlations (r values of each EEG electrode) were shown in panel C both for DAN (upper scalp maps) and DMN (lower scalp maps) stimulation with 100ms moving windows before (-100 – 0ms) and after (1 to 700ms) TMS. Panel D show global mean of test re-test correlations at each time window (Color coded to match scalp maps shown in panel C), for DAN (green bars with standard errors) and DMN (red bars with standard errors).

Movie SV_1 (separate file). Propagation of TMS induced brain activity within the DMN.

Movie SV_2 (separate file). Propagation of TMS induced brain activity within the DAN.

References

1) Alves, L., Simões, M.R., Martins, C., Freitas, S., Santana, I., 2013. Premorbid IQ influence on screening tests' scores in healthy patients and patients with cognitive impairment. J. Geriatr. Psychiatry Neurol. 26, 117–126.
2) Berg, J.-L., Durant, J., Banks, S.J., Miller, J.B., 2016. Estimates of premorbid ability in a neurodegenerative disease clinic population: comparing the Test of Premorbid Functioning and the Wide Range Achievement Test. Clin. Neuropsychol. 30, 547–557.
3) Casarotto, S., Canali, P., Rosanova, M., Pigorini, A., Fecchio, M., Mariotti, M., Lucca, A., Colombo, C., Benedetti, F., Massimini, M., 2013. Assessing the effects of electroconvulsive therapy on cortical excitability by means of transcranial magnetic stimulation and electroencephalography. Brain Topogr. 26, 326–337.
4) Jannati, A., Block, G., Oberman, L.M., Rotenberg, A., Pascual-Leone, A., 2017. Interindividual variability in response to continuous theta-burst stimulation in healthy adults. Clin. Neurophysiol. 128, 2268–2278. https://doi.org/10.1016/j.clinph.2017.08.023
5) Raven, J.C., Court, J.H., 1998. Raven's progressive matrices and vocabulary scales. Oxford pyschologists Press.
6) Santarnecchi, Muller, T., Rossi, S., Sarkar, A., Polizzotto, N.R., Rossi, A., Cohen Kadosh, R., 2016. Individual differences and specificity of prefrontal gamma frequency-tACS on fluid intelligence capabilities. Cortex 75, 33–43. https://doi.org/10.1016/j.cortex.2015.11.003
7) Santarnecchi, Polizzotto, N.R., Godone, M., Giovannelli, F., Feurra, M., Matzen, L., Rossi, A., Rossi, S., 2013. Frequency-Dependent Enhancement of Fluid Intelligence Induced by Transcranial Oscillatory Potentials. Curr. Biol. 23, 1449–1453. https://doi.org/10.1016/j.cub.2013.06.022